Earthquakes and Structures, *Vol. 16, No. 4 (2019) 415-423*
DOI: https://doi.org/10.12989/eas.2019.16.4.415

Use of near-fault pulse-energy for estimating critical structural responses

Zhiwang Chang[1], Zhanhui Liu[*1], Zhenhua Chen[1] and Changhai Zhai[2,]

[1]*School of Civil Engineering, Southwest Jiaotong University, Chengdu 610031, P.R. China*
[2]*School of Civil Engineering, Harbin Institute of Technology, Harbin 150090, P.R. China*

(Received December 30, 2018, Revised February 28, 2019, Accepted March 3, 2019)

Abstract. Near-fault ground motions can impose particularly high seismic demands on structures due to the pulses that are typically observed in the velocity time-histories. In this study it is empirically found that the critical response can be estimated from the directions corresponding to the maximum (max) or minimum (min) pulse-energy. Determination of the pulse-energy requires removing of the high-frequency content. For achieving this, the wavelet analysis and the least-square-fitting (LSF) algorithm are adopted. Results obtained by the two strategies are compared and differences between them are analyzed. Finally, the relationship between the critical response and the response derived from directions having the max or min pulse-energy confirms that using the pulse-energy for deriving the critical response of the building structures is reasonable.

Keywords: near-fault; pulse-like; ground motions; pulse-energy; critical response

1. Introduction

Seismic behavior and consequent damage of a structure can be strongly influenced by its location relative to the ruptured earthquake fault. When the structure is located within an area close to the seismic fault, e.g., within 30 km (Iervolino and Cornell 2008), particularly high seismic demands are usually imposed (Feng *et al.* 2018, Losanno *et al.* 2017). Usually the earthquake ground motions are recorded and orthogonally decomposed along two horizontal directions and one vertical direction. For some critical structures, it is necessary to determine the responses over all possible directions and design for the largest or critical response. According to the guidelines of the ASCE/SEI 7-10 Chapter 16 (2010), the horizontal pair of ground motions shall be rotated to the FN (FP) directions for deriving the most critical response of those structures located at near-fault sites. This is based on the assumption that the FN (FP) component is the severest and would lead to the most critical response over all directions. In the ASCE/SEI 7-10, the use of the maximum-direction (MD) ground motion is prescribed as an additional provision, and it is defined as the direction of a rotated ground motion pair that produces the maximum linear response of an oscillator (ASCE 2010).

Presumably the provision of using the FN (FP) component is due to the knowledge that in near-fault regions, the pulse effects resulted from the forward directivity are generally significant in the FN direction but weak in the FP direction; while the reason of using the MD ground motion is simply in its definition. The guidance documents (e.g., ASCE/SEI 7-10, NIST 2011, BSSC 2015) are meant to be generally applicable to a wide variety of sites and do a good job of accounting for the average case. Since the occurrence of pulse-like motions depends on the geometry of the site and the fault (e.g., Iervolino and Cornell 2008, Shahi and Baker 2011), it may not be suitable to apply the FN (FP) direction in all site-specific cases. Heyden *et al*. (2014) once used the isochrones directivity predictor (IDP) (Spudich and Chiou 2008) to examine the preferred orientation, and they concluded that although the forward-directivity-induced pulses on average tend to be orientated along the FN direction, uncertainty usually exists with regard to the orientation of any single motion. Several other studies (Kalkan and Kwong 2013, Reyes and Kalkan 2015a, Reyes and Kalkan 2015b) also draw similar conclusions that, for a given ground motion pair, the use of the FN (FP) or MD direction does not always yield conservative nonlinear responses. This is because the pulse effects are not always produced in the FN direction, and the MD direction suitable for maximum *elastic* response may be different from the direction for the maximum *inelastic* response.

The objective of this study is to investigate the ability of using the pulse-energy as an indirect parameter for determining the critical response. Here the ground motion energy is mathematically represented by the time integral of the squared ground velocities. It should be noted that it is the velocity-pulses that are considered here since the pulses are typically observed in the velocity time-histories (e.g., Baker 2007, Iervolino and Cornell 2008). The pulses can also occur in the acceleration and displacement time-histories (e.g., Chang *et al.* 2019a, 2019b), however, these are beyond the scope of this study. The bulk of difficulties in deriving the pulse-energy results from the interference of those high-frequency content which hinder a clear picture of the potential pulse. For removing those high-frequency content, two different pulse-extracting strategies are taken here: the wavelet analysis and the least-square-fitting (LSF) algorithm. The pulse-energy is

∗Corresponding author, Ph.D.
E-mail: liuzhanhui@swjtu.edu.cn

http://www.techno-press.com/journals/eas&subpage=7
ISSN: 2092-7614 (Print), 2092-7622 (Online)

discussed by rotating the two horizontal components over a series of evenly distributed directions. The results obtained by the two strategies are compared and differences between them analyzed. Finally, the relationship between the critical response and the response derived from directions having the max (min) pulse-energy is discussed with respect to a simplified reinforced concrete (RC) frame structure. Such a relationship is empirically confirmed reasonable; and the pulse-energy is considered desirable for indirectly deriving the response envelope of the engineered structures of interest. Since only this typical RC frame structures are tested, the related findings shall currently be limited to similar structures and within the employed ground motion samples, and further investigation is warranted concerning its applicability to other structures.

2. Determination of the pulse-energy

A mathematical expression of the pulse-energy involves a clear definition of the pulse-starting and -ending time points on the time axis. Here the peak-point-method (PPM) is preferred for achieving this because it provides a clear definition of the pulse period, and the two local peaks or troughs such defined can be used as the pulse-starting and -ending time points (Zhai *et al.* 2013a). Before achieving this, there is a need of extracting the predominant pulse by removing the high-frequency content.

In this study, extraction of the pulse is realized by the wavelet analysis and the LSF algorithm (Zhai *et al.* 2013a), although there are some alternative ways, like the one in Xu and Agrawal (2010). For the former, detailed technical information can be found in Baker (2007); while for the latter, the pulse model in Dickinson and Gavin (2011) is adopted, and it is mathematically defined as

$$v_{\mathrm{p}}(t;V_{\mathrm{p}},T_{\mathrm{p}},N_{\mathrm{c}},T_{\mathrm{pk}},\varphi)=V_{\mathrm{p}}\exp[-\frac{\pi^2}{4}(\frac{t-T_{\mathrm{pk}}}{N_{\mathrm{c}}T_{\mathrm{p}}})^2] \times\cos(2\pi\frac{t-T_{\mathrm{pk}}}{T_{\mathrm{p}}}-\varphi) \tag{1}$$

where v_{p} is the extracted predominant pulse; t represents the time series; A_{p} denotes the amplitude of the predominant pulse; T_{p} is the pulse period defined by PPM; N_{c} indicates the number of cycles in the pulse, taking a value of 1 for a single pulse; T_{pk} stands for the time location of A_{p}; φ represents the phase of the pulse, generally taking a value of zero. The pulse model, v_{p}, is determined under the condition of minimizing an indicator of α that is formulated by

$$\alpha(T_{\mathrm{p}})=\sum_{i=1}^{n}\left[v(i)-v_p(i;T_p)\right]^2 \tag{2}$$

where n corresponds to the number of the total data points within the original time-history.

Since forward-directivity-induced pulse typically contains one or two significant cycles (Bray and Rodriguez-Marek 2004), and in this study it is the predominant pulse that is considered. The number of significant cycles (N_{c}) is thus set equal to 1, meaning only one single pulse is taken into account. Yet it is worth noting that the pulse number is also considered important to the structural performance since large number of significant pulses can generally cause much severe cumulative seismic damage on the structures. During the pulse extraction, the phase effect is not seen as that important, and thus is ignored, meaning that φ is naturally equal to 0. The parameters of A_{p} and T_{pk} can be readily derived from the predominant pulse, which is defined by the half-circle pulse having the largest energy. For obtaining an extracted pulse that best approximates the pulse in the original motion, the pulse period T_{p} is assumed within a range of 0.1 to 15, and its discrete values increase from 0.1 to 15 at an interval of 0.1. Accordingly, for each of the interested ground motion, 150 resultant pulse time series are produced to match the original velocity time-history. The one with the smallest sum of squared residuals (α) is taken as the optimal extracted pulse, during which the pulse period T_{p} is derived without ambiguity. What should be noted is, taking φ equal to 0 and a maximum value of 15 for T_{p} is confirmed in Zhai *et al.* (2013a) to be able to account for most the of pulse motions that are available in the NGA database (Chiou *et al.* 2008). In addition, using the pulse model in Dickinson and Gavin (2011) is not the unique way for pulse extraction. For example, the pulse model proposed in He and Agrawal (2008) can be taken as an alternative; Kardoutsou *et al.* (2017) recently proposed to determine the predominant pulse by applying the method in Mimoglou *et al.* (2014), among which the Mavroeidis and Papageorgiou pulse model (2003) was adopted.

After extracting the pulse of the original ground motion, the pulse-starting and -ending time can then be used for deriving the pulse-energy, which is defined in a relative sense and determined as the ratio of the energy contained in the predominant pulse to the total seismic energy; and it is mathematically expressed as

$$E=\frac{E_{\mathrm{p}}}{E_{\mathrm{t}}}=\frac{\int_{t_{\mathrm{s}}}^{t_{\mathrm{e}}}v^2(\mathrm{t})\,\mathrm{dt}}{\int_0^{\infty}v^2(\mathrm{t})\,\mathrm{dt}} \tag{3}$$

where t_{s} and t_{e} represent the pulse-starting and -ending points on the time axis, respectively; $v(t)$ indicates the velocity time-history of the original ground motion.

3. Differences between the two pulse-extracting strategies

Both the wavelet analysis and the LSF algorithm can be used for removing the high-frequency content and extracting the velocity-pulse. Here the differences between the two methods are interpreted by observing the pulse-like features after rotating the horizontal ground motion pair over a range of directions. The method proposed in Zhai *et al*. (2013a) permits the range of these pulse-like and non-pulse-like directions to be visualized in a quantitative way. For illustration, a typical ground motion component, the Pacoima Dam (upper left abutment) ground motion (hereafter abbreviated as the PDGM record) recorded in the 1971 San Fernando earthquake, is employed here. Forty pulse energies are calculated and displayed in Fig. 1 after

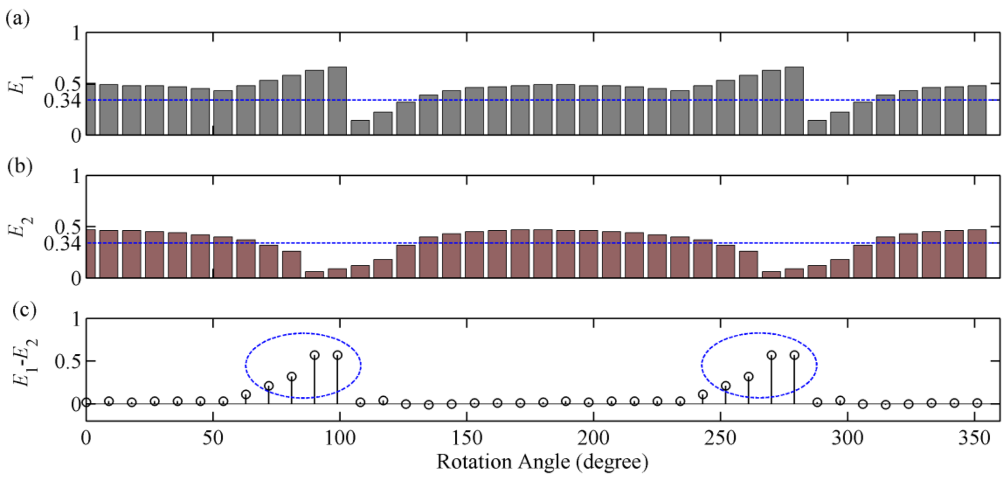

Fig. 1 Pulse-energy obtained through (a) the wavelet analysis and (b) the LSF algorithm along 40 orientations; (c) the pulse-energy difference between the two ways of pulse-extracting methods.

rotating its two horizontal components from 0° to 351° at every 9°, with the 0° direction indicating the FN direction. Fig. 1(a) presents the pulse-energy (E_1) corresponding to the wavelet-analysis-extracted pulses, while Fig. 1(b) corresponding to the LSF-extracted results (E_2); Fig. 1(c) shows the energy differences by the two ways of pulse extraction. After comparison, it is found that most of the pulse-energy derived by the two methods are equal or nearly equal. Yet there are four directions in which great differences exist: 72°, 81°, 90° and 99°. (Note waveforms are similar for the rotated components at the directions of θ and θ+180° due to symmetry). In these particular directions, the pulse-energy, E_1, exceed the pulse-detecting threshold level of 0.34 determined in Chang *et al.* (2016); while the values of E_2 clearly fall below this threshold.

So why, in the above direction, is there a significant divergence between the results derived by the two pulse-extracting methods? To investigate such an issue, the velocity time-histories as well as the extracted pulses of the PDGM record rotated over 20 azimuths from 9° to 180° are computed and exhibited in Fig. 2. The extracted pulses in the left column are from the wavelet analysis while those in the right column are from the LSF algorithm. After comparing the extracted pulses in Fig. 2, it is found that within most of the azimuth range the potential pulses extracted by the two approaches coincide well with each other. However, in the previous particular directions between 72° and 99° (including 63°), the predominant pulses derived from the wavelet analysis significantly differ from those obtained by the LSF algorithm. The potential pulses extracted by the former appear as waveforms comprising multiple spikes; while the pulses derived from the latter emerge as single bumps. The reason behind such a divergence is that in the LSF algorithm, the number of pulse cycles, N_c, is here always assumed taking a value of 1; that is, only one predominant pulse is considered within a ground motion. However, the wavelet analysis is believed to identify a region with high energy as where the predominant velocity-pulse locates. In case of ground motions with significant pulses, this region generally includes a single dominant pulse; while in ground motions with non-typical pulses, this region may consist of a series of multiple spikes that are in nature non-pulse-like, see Fig. 2.

One possible technical reason for explaining the above limitation of using the wavelet analysis is that the pulse-extracting procedure in Baker (2007) only counts on the largest coefficient to detect pulse-like features. For some ground motions, a wavelet other than the largest one can be dominant in the ground motion. To avoid such a situation, Shahi and Baker (2014) proposed an improved algorithm using five nonadjacent potential pulses for the purpose of classification, and the ground motion is considered as pulse-like if any of the five potential pulses can be detected as pulse-like. This practice is confirmed capable of greatly improving the efficiency of using the wavelet analysis for extracting a 'true' pulse. In spite of this, the wavelet analysis in Baker (2007) is still widely used worldwide; thus, it is recommended here that the Shahi and Baker (2014), as an updated version of the Baker (2007), should be used if the wavelet analysis is considered as an alternative for extracting pulse.

4. Use of the pulse-energy for estimating critical response

The velocity-pulses are generally interpreted as a region containing high seismic energy. If inputted into the structure, large pulse-energy is required to be dissipated in a single or relatively few cycles, causing large or excessive seismic demands in a short-time interval (Kalkan and Kunnath 2006). This implies that a potential relation exists between the pulse-energy and the resulted engineering demand parameters (EDP). Such a relationship over non-redundant directions is discussed in this section through a benchmark building model. The model is for a 5-story RC frame structure and has a regular symmetric vertical layout with a first-mode vibration period of 0.89 second; more detailed designing information can be found in Zhai *et al*. (2013b).

As a case study, the 40 rotated acceleration

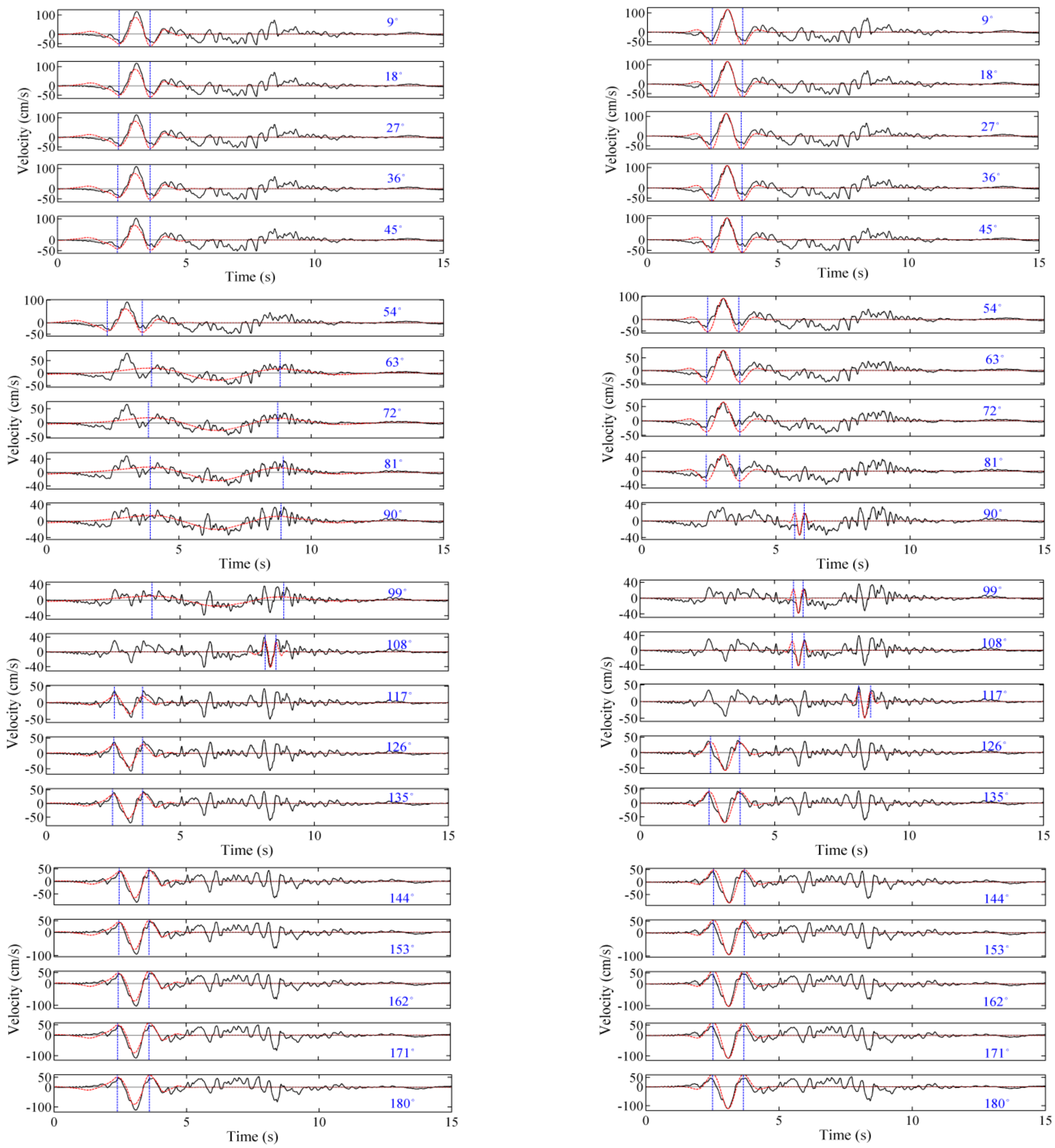

Fig. 2 Velocity time series (in solid line) of NGA0077 rotated over 20 azimuths as well as their extracted potential pulses (in dashed line) obtained from: (left) the wavelet analysis and (right) the LSF algorithm

time-histories of the above PDGM record are first utilized as the excitation inputs in the non-linear dynamic analysis of the benchmark model. The EDP values are evaluated using the computer program IDARC (e.g., Kunnath *et al.* 1992). This program has been widely used by the research community as a platform for nonlinear structural analysis, in which various aspects of concrete behavior can be modeled. The EDPs considered here are the inter-story drift ratio (ISDR) for representing the peak structural response, and the Park & Ang damage index (PADI) to account for the cumulative structural behavior (Park and Ang, 1985). The pulse-energy is calculated from the velocity-pulse derived from the LSF algorithm. The values of the two EDPs against the rotated directions are exhibited in Fig. 3. It can be clearly observed that the orientation-variant trends of the two EDPs are similar to that for the pulse-energy shown in Zhai *et al.* (2013a) (the PDGM record was also used in Zhai *et al*. (2013a) as an exemplified record). The directions along which the critical responses occur agree with the directions that the max (min) pulse-energy are derived. For this particular ground motion, it is in the FN (FP) direction that the critical responses are observed, although it is not always the case for other ground motions (Kalkan and Kwong 2013). The relationships of two EDPs versus the pulse-energy are displayed in Fig. 3(c) and (d). It is apparent that the two quantities correlate well with the pulse-energy. The coefficients of determination, R^2, of the two relationships respectively reach as large as 0.91 and

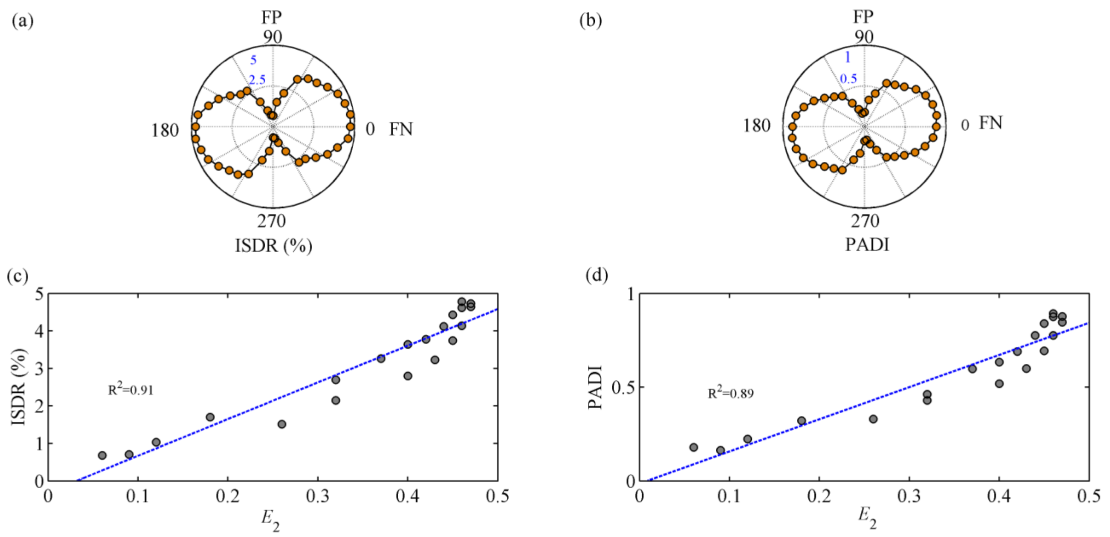

Fig. 3 (a) ISDR and (b) PADI as a function of the seismic incidence azimuth; correlation of: (c) ISDR and (d) PADI with the pulse-energy E_2

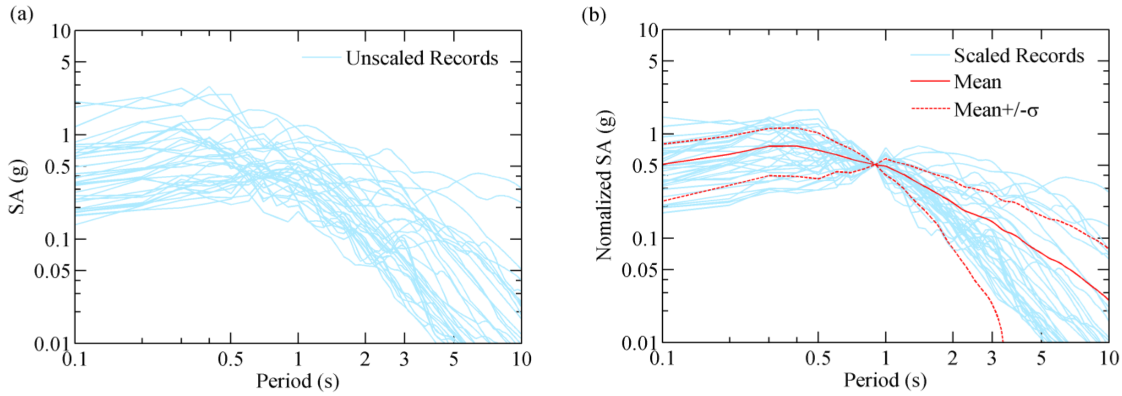

Fig. 4 Pseudo-spectral acceleration of the 17 pairs of: (a) unscaled records and (b) scaled records

0.89, indicating the presence of a strong relation.

To further examine the above relationship, 16 more pairs of as-recorded (real) ground motions are selected and listed in Table 1 (including the above PDGM record assigned to NO.17). All ground motion data can be conveniently downloaded from the NGA-West 2 database (Ancheta *et al.* 2013). The unscaled as well as scaled (normalized by the mean value at the fundamental period, 0.89s, of the benchmark model) pseudo-acceleration spectra are shown in Fig. 4; and the orientation-variant pulse energies are exhibited in Fig. 5 with the 0° azimuth indicating the FN direction. The criteria for compiling such a database are that: the PGVs of at least one of the two as-recorded components exceed 30 cm/s; the unscaled/scaled spectral shapes are overall similar, or no peculiar spectral shapes are observed of the 17 pairs of ground motions; the pulse-energy over at least one of the rotated directions are larger than 0.34, the threshold level in Chang *et al.* (2016) for identifying the presence of a strong pulse feature (see Fig. 5). It can be also found in Fig. 5 that, although the FN direction clearly shows the pulse-like feature for most of the 16 pairs of ground motions, yet the most significant pulse-like features are not necessarily observed along this direction, or for some ground motions (like the NO. 16 ground motion), even non-pulse-like features occur in the FN direction. Again, this proves that it is not desirable of resorting to the FN (FP) direction for deriving the most critical response.

To empirically justify the use of pulse-energy in deriving the critical response, the 17 rotated unscaled ground motions are used as the inputs for dynamic analysis. For each ground motion pair, 20 azimuths are considered, from the 0° to the 171° at every 9°; that is, 340 dynamic analyses (including those for the PAGM record) are performed. Hereafter for convenience, the subscripts of maxE (minE) are used to represent the directions where the max (min) pulse energy occur over the 20 azimuths.

In order to give comparable results, the structural damage indices (ISDR and the PADI) to the components along the FN and FP orientations are then calculated and shown in Figs. 6-7. The solid and hollow circles represent the EDPs derived from the directions in which the max and min pulse-energy are calculated; while the solid and hollow triangles indicate the EDPs computed from the FN and FP orientations.

In Fig. 6, it is clearly found that the EDPs along the maxE (minE) directions are much closer to the max (min) EDPs, compared with the ones along the FN (FP)

Table 1 Basic information of the 17 pairs of pulse-like ground motions used in this study

Record NO.	Earthquake Event	Year	Strike (°)	Station	Component	PGV (cm/s)	E_2
1	Taiwan Smart1 (40)	1986	43	Smart1-C00	40C00EW	33	0.48
					40C00NS	19	0.36
2	Taiwan Smart1 (40)	1986	43	Smart1-E01	40E01EW	36	0.60
					40E01NS	15	0.15
3	Taiwan Smart1 (40)	1986	43	Smart1-I01	40I01EW	32	0.53
					40I01NS	18	0.37
4	Taiwan Smart1 (40)	1986	43	Smart1-I07	40I07EW	31	0.43
					40I07NS	18	0.31
5	Taiwan Smart1 (40)	1986	43	Smart1-M07	40M07EW	38	0.62
					40M07NS	24	0.56
6	Erzincan	1992	122	Erzincan	ERZ-EW	64	0.37
					ERZ-NS	84	0.69
7	Kocaeli	1999	272	Gebze	GBZ000	50	0.66
					GBZ270	30	0.68
8	Loma Prieta	1989	128	Gilroy Historic Bldg	GOF090	42	0.49
					GOF180	24	0.27
9	Imperial Valley	1979	323	EC Meloland Overp FF	H-EM0000	72	0.68
					H-EM0270	90	0.68
10	Loma Prieta	1989	128	Presidio	PRS000	13	0.23
					PRS090	32	0.48
11	Northridge	1994	122	Stone Canyon	SCR000	28	0.32
					SCR090	38	0.42
12	Loma Prieta	1989	128	Palo Alto Slac Lab	SLC270	37	0.31
					SLC360	29	0.41
13	Northridge	1994	122	Sepulveda VA	SPV270	85	0.41
					SPV360	76	0.09
14	Chi-Chi	1999	5	TCU068	TCU068-N	263	0.78
					TCU068-W	176	0.79
15	Chi-Chi	1999	5	TCU075	TCU075-N	38	0.25
					TCU075-W	88	0.70
16	Chi-Chi	1999	5	TCU076	TCU076-N	64	0.17
					TCU076-W	63	0.34
17	San Fernando	1971	287	Pacoima Dam (upper left abutment)	PUL164	112	0.45
					PUL254	54	0.30

orientation. Although in some cases the EDPs in the FN (FP) orientation coincide with the max (min) EDPs, in most cases presented above, the FN (FP) direction only shows weak correlation with the critical response. It can be also found that all the EDPs along the maxE direction are larger than that along the minE direction with regard to the two interested EDPs. Yet, the EDPs along the FP orientation are in some cases larger than that along the FN orientation. Since we'd like to use the pulse-energy for enveloping the structural response over all directions, it is better to examine this ability by using the ratio of the EDP difference along the interested directions to the EDP difference between the max and the min EDPs; that is

$$R_{\mathrm{EDP\text{-}1}} = \frac{\mathrm{EDP}_{\mathrm{maxE}} - \mathrm{EDP}_{\mathrm{minE}}}{\mathrm{EDP}_{\max} - \mathrm{EDP}_{\min}} \tag{4}$$

$$R_{\mathrm{EDP\text{-}2}} = \frac{\mathrm{EDP}_{\mathrm{FN}} - \mathrm{EDP}_{\mathrm{FP}}}{\mathrm{EDP}_{\max} - \mathrm{EDP}_{\min}} \tag{5}$$

in which, $R_{\mathrm{EDP\text{-}1}}$ represents the ratio of the EDP difference along the maxE and minE directions to the difference between the max and the min EDPs; while $R_{\mathrm{EDP\text{-}2}}$ indicates the ratio of the EDP difference along the FN and FP directions to the difference between the max and the min EDPs. The related results for the two ratios are illustrated in Fig. 7. It is apparent that the response range enveloped using the maxE and minE directions are much better than that using the FN and FP orientations, since the $R_{\mathrm{EDP\text{-}1}}$ values are overall larger than the $R_{\mathrm{EDP\text{-}2}}$ values and are much closer to 1. The mean value of the former is 0.63 (0.66) in contrast to 0.07 (0.09) of the latter for the two interested EDPs.

5. Discussions and Conclusions

The velocity-pulses in near-fault ground motions are believed to contain a concentrated seismic energy, which might impose a great seismic demand on the structures. For deriving the pulse-energy, two different strategies are taken to extract the velocity-pulse: one by the wavelet analysis, the other by the LSF algorithm. Results obtained by the two strategies are compared and differences between them

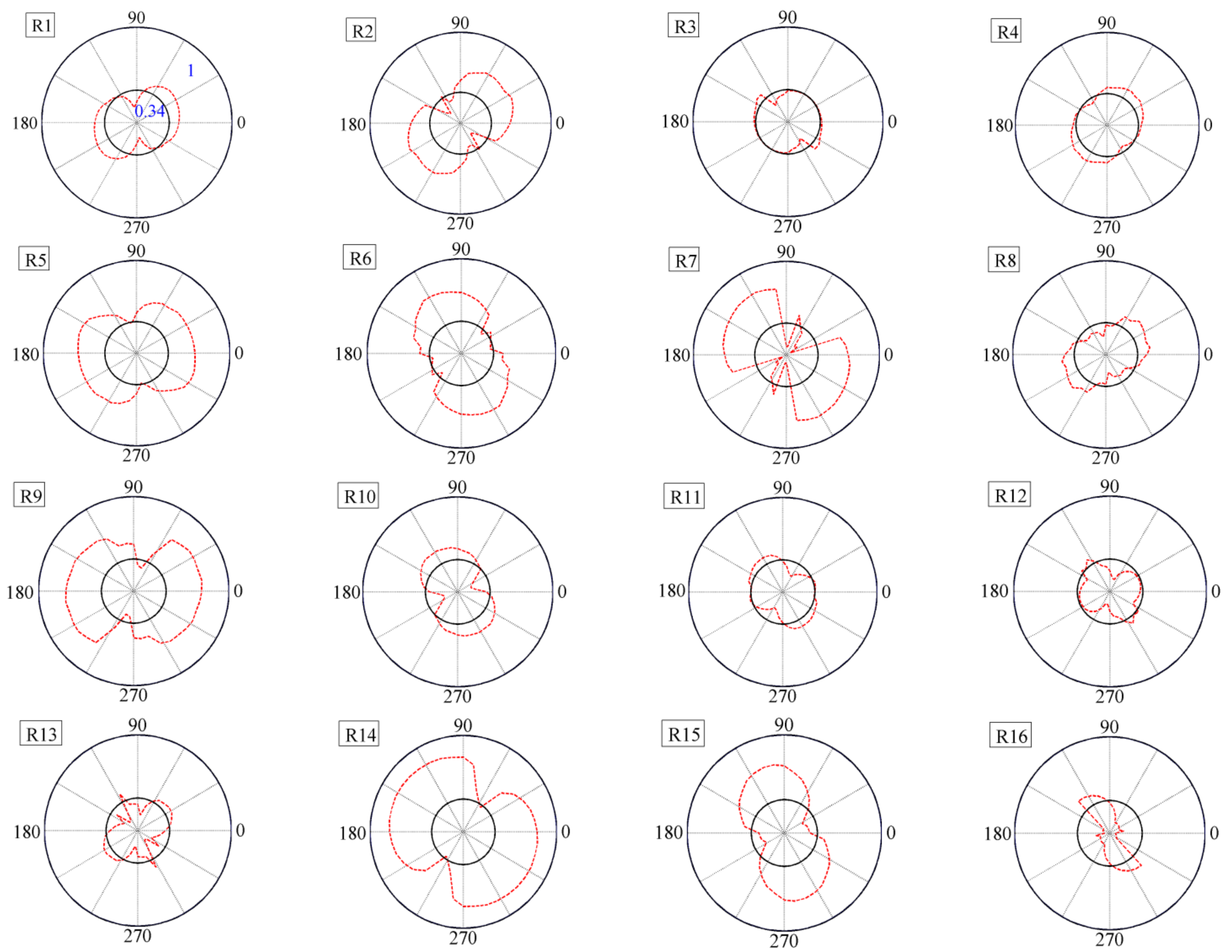

Fig. 5 Pulse-like features of the 16 pairs of ground motions rotated over all directions; the 0° indicates the FN direction; the inner solid circle represents the threshold level of 0.34 used for identifying the presence of significant pulses

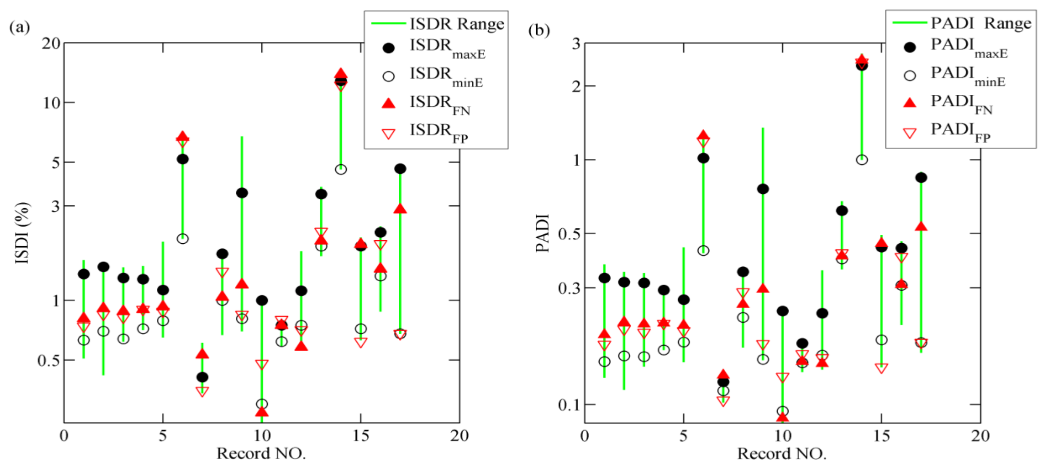

Fig. 6 Response range of: (a) ISDR and (b) PADI for the 17 pairs of ground motions; The solid and hollow circles represent the EDPs derived from the directions in which the max and min pulse energies are calculated; while the solid and hollow triangles indicate the EDPs computed from the FN and FP orientations

analyzed. When there is a single dominant pulse, both of the two strategies can be considered as reliable approaches. However, when it comes to some non-pulse-like ground motions, the potential pulse extracted by the wavelet analysis in Baker (2007) is likely to be comprised of a series of multiple non-pulse-like spikes; while the LSF algorithm as a way of pulse-extraction preferably avoids such a situation. Nevertheless, the Shahi and Baker (2014), as an updated version of the Baker (2007), could be used an alternative if the wavelet analysis is considered as a way for

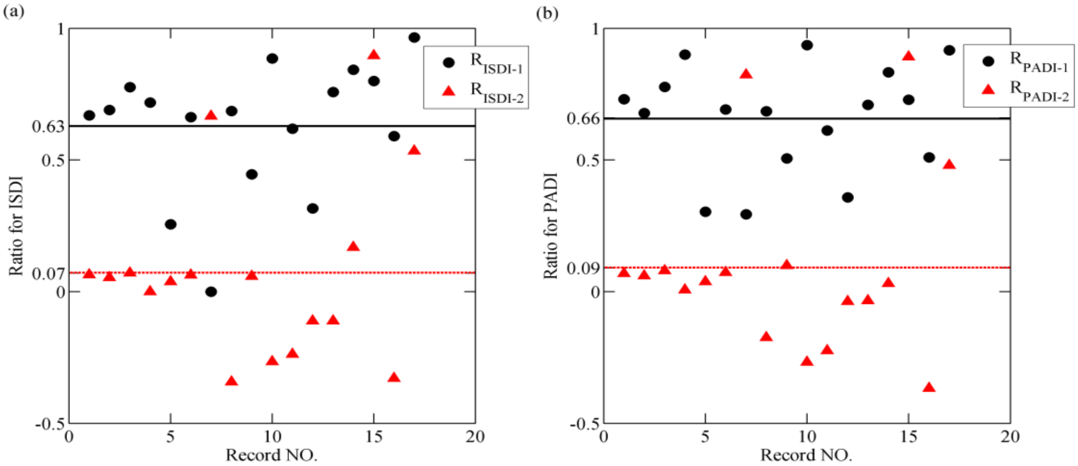

Fig. 7 The ratio of the EDP difference along the interested directions to the EDP difference between the max and the min EDPs for: (a) ISDR and (b) PADI; The solid and circles represent the ratio of the EDP difference along the maxE and minE directions to the difference between the Max and the Min EDPs; while the solid triangles indicate ratio of the EDP difference along the FN and FP directions to the difference between the max and the min EDPs

extracting pulse.

The practice of using the FN (FP) direction for deriving the critical response is generally applicable to earthquake scenarios, but it is not necessarily to produce the max (min) response for any ground motions. The pulse-energy is proposed as an indirect way for estimating the critical response. It is confirmed with respect to a generic benchmark model that the response range enveloped using the maxE and minE directions are much better than that using the FN and FP orientations. In future studies, there are some issues that should be further investigated. In an ideal condition, verification of the new parameter must be thoroughly conducted by analyzing all the damage states for all kinds of building structures with numerous seismic records. This is of course physically impossible. There are so many factors influencing the structural behaviors (including the properties of the seismic inputs and the structure itself) that it is equally rather difficult to consider all factors in a single article. For the time being this study just tested the proposed indicator (the pulse-energy) with a low-rise RC frame structure. The structure represents a series of typical buildings that are commonly used in China. The author wants the tested building to have an overall generic behavior as much as possible, while disregards those specific characteristics for individual systems. The reason is based on the fact that the more complex a structure is, the more factors that are to be considered, and thus, the more difficult the true controlling factors can be found. Nevertheless, since only this low-rise RC structure is tested, the corresponding findings shall currently be only limited to similar low-rise RC structures as well as within the employed ground motion samples, and its applicability to other structures needs further work in future studies.

Acknowledgments

This study is financially supported by the National Key Research and Development Program of China (2016YFB1200401), the National Natural Science Foundation of China (NO. 51708461), the Fundamental Research Funds for the Central Universities (NO. 2682016CX010, 2682016CX013), the Scientific Research Projects for Building High-level Faculty in Southwest Jiao Tong University (NO. 10101X10096077). Zhanhui Liu and Zhiwang Chang would like to express their special acknowledgments to the *China Scholarship Council* for the financial support during their research stay in UK. The authors want to thank Prof. Jack W. Baker for the computer programs. Strong ground motions were obtained from the Pacific Earthquake Engineering Research Center database (last accessed September 2018).

References

American Society of Civil Engineers (ASCE) (2010), Minimum Design Loads for Buildings and Other Structures, ASCE/SEI 7-10, Reston, VA.

Ancheta, T.D., Darragh, R.B., Stewart, J.P., Seyhan, E., Silva, W.J., Chiou, B,S.J., Wooddell, K.E., Graves, R.W., Kottke, A.R., Boore, D.M., Kishida, T. and Donahue, J.L. (2013), "NGA-West2 database", *Earthq. Spectra*, **30**(3), 989-1005.

Baker, J.W. (2007), "Quantitative classification of near-fault ground motions using wavelet analysis", *Bull. Seismol. Soc. Am.*, **97**(5), 1486-1501.

Bray, J.D. and Rodriguez-Marek, A. (2004), "Characterization of forward directivity ground motions in the near-fault region", *Soil Dyn. Earthq. Eng.*, **24**(11), 815-828.

BSSC (2015), NEHRP Recommended Seismic Provisions for New Buildings and Other Structures, FEMA P-1050, Building Seismic Safety Council, Washington, D.C.

Chang, Z., De Luca, F. and Goda, K. (2019a), "Automated classification of near-fault acceleration pulses using wavelet packets", *Comput. Aid. Civil Infrastr. Eng.*, DOI: 10.1111/ mice.12437.

Chang, Z., De Luca, F. and Goda, K. (2019b), "Near-fault acceleration-pulses and non-acceleration-pulses: Effects on the inelastic displacement ratio", *Earthq. Eng. Struct. Dyn.*. (under Review)

Chang, Z., Sun, X., Zhai, C., Zhao, J. X. and Xie, L. (2016), "An improved energy-based approach for selecting pulse-like ground motions", *Earthq. Eng. Struct. Dyn.*, **45**, 2405-2411.
Chiou, B., Darragh, R., Gregor, N. and Silva, W. (2008), "NGA project strong-motion database", *Earthq. Spectra*, **24**(1), 23-44.
Dickinson, B. and Gavin, H. (2011), "Parametric statistical generalization of uniform-hazard earthquake ground motions", *J. Struct. Eng.*, **137**(3), 410-422.
Feng, R., Chen, Y. and Cui, G. (2018), "Dynamic response of post-tensioned rocking wall-moment frames under near-fault ground excitation", *Earthq. Struct.*, **15**(3), 243-251.
Hayden, C., Bray, J. and Abrahamson, N. (2014), "Selection of near-fault pulse motions", *J. Geotech. Geoenviron. Eng.*, **140**(7), 04014030.
He, W.L. and Agrawal, A.K. (2008), "Analytical model of ground motion pulses for the design and assessment of seismic protective systems", *J. Struct. Eng.*, **134**(7), 1177-1188.
Iervolino, I. and Cornell, C.A. (2008), "Probability of occurrence of velocity pulses in near-source ground motions", *Bull. Seismol. Soc. Am.*, **98**(5), 2262-2277.
Kalkan, E. and Kunnath, S. (2006), "Effects of fling step and forward directivity on seismic response of buildings", *Earthq. Spectra*, **22**(2), 367-390.
Kalkan, E. and Kwong, N. (2013), "Pros and cons of rotating ground motion records to fault-mormal/parallel directions for response history analysis of buildings", *J. Struct. Eng.*, **140**(3), 04013062.
Kardoutsou, V., Taflampas, I. and Psycharis, I.N. (2017), "A new pulse indicator for the classification of ground motions", *Bull. Seismol. Soc. Am.*, **107**(3), 1356-1364.
Kunnath, S.K., Reinhorn, A.M. and Lobo, R.F. (1992), "IDARC Version 3.0: A program for the inelastic damage analysis of reinforced concrete structures", Report No. NCEER-92-0022, National Center for Earthquake Engineering Research, University at Buffalo, the State University of New York.
Losanno, D., Hadad, H.A. and Serino, G. (2017), "Seismic behavior of isolated bridges with additional damping under far-field and near fault ground motion", *Earthq. Struct.*, **13**(2), 119-130.
Mavroeidis, G.P. and Papageorgiou, A.S. (2003), "A mathematical representation of near-fault ground motions", *Bull. Seismol. Soc. Am.*, **93**(3), 1099-1131.
Mimoglou, P., Psycharis, I.N. and Taflampas, I.M. (2014), "Explicit determination of the pulse inherent in pulse-like ground motions", *Earthq. Eng. Struct. Dyn.*, **43**, 2261-2281.
NIST (2011), Selecting and Scaling Earthquake Ground Motions for Performing Response-History Analyses, NIST GCR 11-917-15, Prepared by the NEHRP Consultants Joint Venture for the National Institute of Standards and Technology, Gaithersburg, Maryland.
Park, Y. and Ang, A. (1985), "Mechanistic seismic damage model for reinforced concrete", *J. Struct. Eng.*, **111**(4), 740-757.
Reyes, J. and Kalkan, E. (2015a), "Significance of rotating ground motions on behavior of symmetric- and asymmetric-plan structures-Part I. Single-story structures", *Earthq. Spectra*, **31**(3), 1591-1612.
Reyes, J. and Kalkan, E. (2015b), "Significance of rotating ground motions on behavior of symmetric- and asymmetric-plan structures-Part II. Multi-story structures", *Earthq. Spectra*, **31**(3), 1613-1628.
Shahi, S. and Baker, J. (2011), "An empirically calibrated framework for including the effects of near-fault directivity in probabilistic seismic hazard analysis", *Bull. Seismol. Soc. Am.*, **101**(2), 742-755.
Shahi, S. and Baker, J. (2014), "An efficient algorithm to identify strong-velocity pulses in multicomponent ground motions", *Bull. Seismol. Soc. Am.*, **104**(5), 2456-2466.
Spudich, P. and Chiou, B.S.J. (2008), "Directivity in NGA earthquake ground motions: Analysis using isochrone theory", *Earthq. Spectra*, **24**(1), 279-298.
Xu, Z. and Agrawal, A. (2010), "Decomposition and effects of pulse components in near-field ground motions", *J. Struct. Eng.*, **136**(6), 690-699.
Zhai, C., Chang, Z., Li, S. and Xie, L. (2013b), "Selection of the most unfavorable real ground motions for low-and mid-rise RC frame structures", *J. Earthq. Eng.*, **17**, 1233-1251.
Zhai, C., Chang, Z., Li, S., Chen, Z. and Xie, L. (2013a), "Quantitative identification of near-fault pulse‐like ground motions based on energy", *Bull. Seismol. Soc. Am.*, **103**(5), 2591-2603.

AT